RESEARCH ARTICLE

Analysis and Compensation of Phase Shift Errors of an Open-Loop Current Transducer Considering Eddy Current

KISEOK KIM[1], **(Graduate Student Member, IEEE), YOONJAE KIM**[2], **(Member, IEEE), JI-HOON HAN**[1], **(Graduate Student Member, IEEE), AND SUN-KI HONG**[3], **(Member, IEEE)**

[1]Department of Information Control Engineering, Hoseo University, Asan 31499, Republic of Korea
[2]Department of Electrical Engineering, Hoseo University, Asan 31499, Republic of Korea
[3]Department of System and Control Engineering, Hoseo University, Asan 31499, Republic of Korea

Corresponding author: Sun-Ki Hong (sunkih4@naver.com)

ABSTRACT The open-loop current transducer comprises a magnetic core made of soft magnet material and includes a Hall sensor. Traction motors in applications such as electric vehicles tend to be driven at high speeds. It pushes the inverters to increase the fundamental frequency of the output current above 1 kHz. However, this high frequency current generates eddy currents in the magnetic core of the current transducers. They deteriorate the measurement data thereby resulting the amplitude error and phase shift error, which is applied open-loop current transducer with the lamination magnetic core. In this study, the errors of an open-loop current transducer due to eddy currents were analyzed through mathematical modeling and finite element method (FEM). Furthermore, the impact of the error on permanent magnet synchronous motor current control was studied. The phase shift error of the current transducer used in this study reaches 3.6 degree when the frequency of current was 1.5 kHz, resulting in about a 20% torque reduction during field-weakening operation at 200 kW, 22500 rpm. On the other hand, the amplitude error of the current transducer is only 0.18% in the same condition. In order to correct the error, an online compensation method is proposed based on FEM simulation results. The phase shift error was verified through the experiments with a 300 μH, 3-phase inductive load. The proposed method was also validated through the experimental results conducted for variable frequencies from 500 Hz to 1.5 kHz.

INDEX TERMS Open-loop current transducer, current sensor, magnetic core, electrical sheet, hysteresis, eddy current, traction motor, motor control, vector control, inverter.

I. INTRODUCTION

Current feedback is crucial for motor control in inverters, with various methods employed for current measurement including shunt resistance, current transformers, current transducers, Rogowski coils, and others [1], [2], [3]. This paper focuses on an open-loop current transducer utilizing a C-type magnetic core and a Hall sensor. This transducer

operates by inducing a magnetic field through current measurement on the primary side, with the field concentrated on the C-type magnetic core. An air gap within the core houses the Hall sensor, which detects the magnetic field and outputs it as voltage [4]. Traction motors in applications such as contemporary electric vehicles (EV) often operate at high speeds, necessitating measurement of the higher frequency by the current transducer. However, as the frequency surpasses hundreds of Hz, significant eddy currents arise within the magnetic core, leading to pronounced hysteresis and resulting

phase shift errors. This phenomenon causes the inverter to measure incorrect currents at the same instantaneous value, thereby compromising torque and impeding optimal current control [5]. Consequently, under vector current control, the actual applied current may increase, potentially decreasing the efficiency of the inverter.

To mitigate phase shift errors, options such as employing open-loop current transducers made of powdered magnetic materials or closed-loop and flux gate types are available. Nevertheless, for high-current measurement, environ-mental robustness, and cost-effectiveness, an open-loop current transducer with a simple structure and a highly reliable electrical steel magnetic core is preferred [4].

This paper conducts a thorough analysis of the phase shift error induced by eddy current within the magnetic core, employing mathematical and finite element analysis methods [6]. Through an experiment on the inverter's current control using silicon carbide FET, it is shown that the open-loop current transducer contains a phase shift error that is proportional to frequency when increased to 1.5 kHz. Mathematically, it is established that the phase shift error increases linearly with frequency. When employing vector control, the angular velocity (ω) can be derived from angle feedback and can easily compensate for phase shift errors. Experimental validation confirmed the adequacy of error compensation strategies based on the modeled phase shift error.

II. PHASE SHIFT ERROR OF CURRENT TRANSDUCER
A. OPEN-LOOP TYPE CURRENT TRANSDUCER

A current transducer is a sensor that measures current using an insulating method. It is categorized into three types based on the measurement technique: open-loop, closed-loop, and fluxgate [7], [8]. The current transducer consists of a C-type magnetic core with an air gap, which concentrates the magnetic field generated by the primary current to be measured, creating a high and uniform magnetic field in the air gap. The resultant magnetic field is then measured and converted into a current value, thereby facilitating the measurement of the primary current [4], [5].

An open-loop current transducer utilizes a Hall sensor to convert the magnetic field generated in the magnetic core into voltage. The voltage output of the Hall sensor is expressed as follows (1), where V_h represents the output voltage of the Hall sensor, $\vec{I_c}$ denotes the current flowing within the Hall sensor, and $\vec{B}$ signifies the magnetic flux density passing vertically through the Hall sensor [9].

$$V_h \propto \vec{I_c} \times \vec{B} \qquad (1)$$

With the simplest structure comprising only a magnetic core and a Hall sensor, as shown in Fig. 1, the open-loop current transducer is cost-effective and robust, making it particularly suitable for applications demanding high reliability, such as EV inverters [4], [5].

The magnetic core of the current transducer is composed of soft magnet material with high magnetic permeability. However, the magnetic nonlinearity of the core can introduce
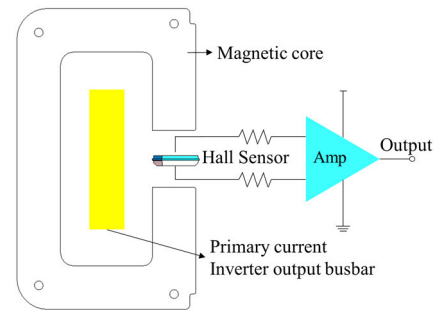

FIGURE 1. Open-loop current transducer structure.

errors in the current transducer's measurements [10], [11]. Therefore, careful material selection is crucial, typically involving the lamination of thin steel plates to mitigate iron loss resulting from eddy currents. In this study, a magnetic core made of 0.35 mm isotropic steel plates was employed. Thinner magnetic core materials result in reduced eddy currents and, consequently, lower current transducer errors. However, cost-effective manufacturing necessitates the use of materials with appropriate thicknesses. Table 1 shows the characteristics of the magnetic core (35PN230) used. Where the iron loss is at 1.5 T and 50 Hz [10], [12].

TABLE 1. Material characteristics of the magnetic core.

Thickness [mm]	Iron loss [W/kg]	Flux density @5kA/m [T]	Resistivity [$\Omega \cdot$ m]
0.35	2.30	1.62	59×10^{-8}

B. EDDY CURRENT OF THE MAGNETIC CORE

Soft magnetic material, which is the magnetic core material, has electrical resistance. It possesses the characteristic of increased coercive force with rising frequency. Fig. 2 shows a hysteresis loop where the coercive force increases as the frequency increases. This characteristic is applied in the magnetic core of the current transducer [5], [13].
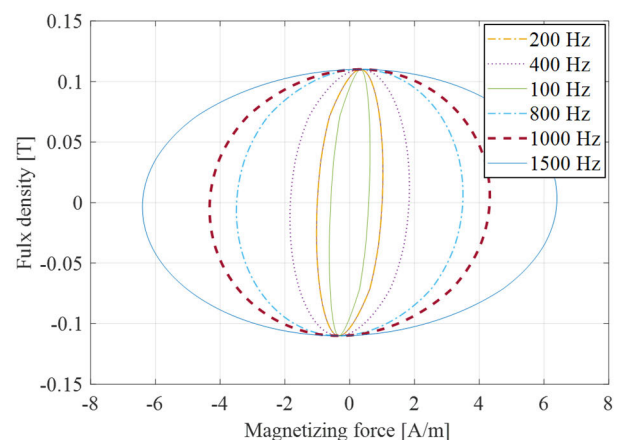

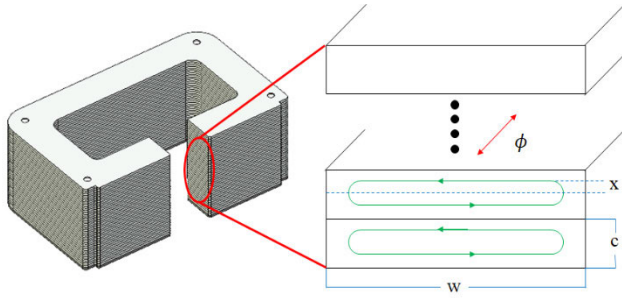**FIGURE 2. Hysteresis loop by the frequency.**

FIGURE 3. Lamination magnetic core and cross section.

FIGURE 4. Phase shift error analysis with and without hysteresis.

Eddy currents are generated in response to alterations in the magnetic field induced by the primary current. As depicted in Fig. 3, injection of the primary current leads to eddy current formation within the magnetic core. Higher frequencies correspond to augmented eddy current generation [5], [13].

The eddy currents generated within the magnetic core are primarily influenced by the electrical resistance of the core material, which varies depending on the material and shape of the core. Eddy currents in the magnetic core are calculated from the current density J_x and are represented by (2).

$$J_x = \frac{E_x}{\rho},\qquad(2)$$

where E_x denotes the electric field intensity, d is the distance to the magnetic core, V_x is the electric potential of the magnetic core, which is expressed as (3).

$$E_x = \frac{V_x}{d} = -\frac{1}{2w}\frac{d}{dt}\phi = -\frac{1}{2w}\frac{d}{dt}(2x \cdot w \cdot B_a)$$
$$= -\frac{d}{dt}(x \cdot B_a),\qquad(3)$$

where x, c, and w denote magnetic core shape, ϕ is the magnetic flux in the core in Fig. 3, B_a is flux density in the magnetic core, ρ is the resistivity of the magnetic core, and current in the magnetic core is expressed as (4).

$$i_{core} = \int_0^{\frac{c}{2}} J_x dA_x = \frac{1}{\rho}\int_0^{\frac{c}{2}} -\frac{d}{dt}(x \cdot B_a) \cdot l_c dx$$
$$= -\frac{l_c}{\rho}\frac{1}{2}\left(\frac{c}{2}\right)^2 \frac{dB_a}{dt}\qquad(4)$$

Equation (4) represents the current in the magnetic core, which can be expressed as an eddy current in the magnetic core equation, as shown in (5), especially when the primary current is sinusoidal. This formulation incorporates magnetic core properties, where N represents the number of magnetic core laminations, k_a is the correction coefficient, B_m is the amplitude of the flux density in the magnetic core, and l_c denotes the length of the magnetic flux path.

$$i_e = -\frac{N \cdot l_c}{k_a \cdot \rho} \cdot \frac{c^2}{8} \cdot B_m \cdot \omega \cos(\omega t)\qquad(5)$$

The hysteresis and eddy current phenomenon cause phase shift error in the current transducer. Following the determination of the magnetic core material, analysis can be
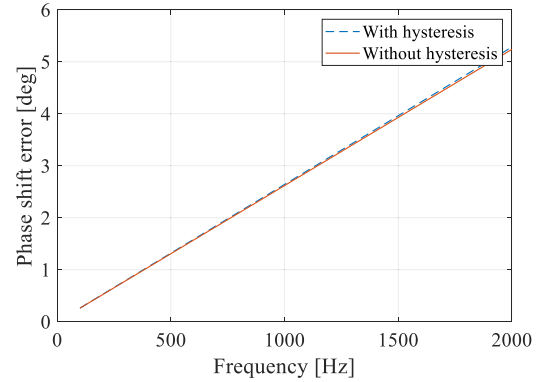
conducted using the Preisach model, a mathematical model. Utilizing nonlinear hysteresis analysis, the magnetic field behavior within the air gap, contingent upon the magnetic core shape, can be computed. Although hysteresis-inclusive analysis enables precise examination, it entails significant computational efforts, thereby prolonging the analysis duration [5], [14]. At low current measurement frequencies, phase shift errors attributable to hysteresis exist but remain minimal. Conversely, at current measurement frequencies, typically hundreds of Hz or higher, phase shift errors due to the eddy current phenomenon surpass those caused by hysteresis, rendering the latter's contribution negligible [5]. Fig. 4 shows the phase shift error resulting from eddy currents within the magnetic core, with and without the presence of hysteresis phenomena.

C. PHASE SHIFT ERROR VERIFICATION
As mentioned previously, the output of an open-loop current transducer includes the component of eddy current. Assuming a-phase current is sinusoidal, the measured current with the eddy current is given by

$$\hat{i}_a = i_a + i_e$$
$$= I_a \sin(\omega t) - \frac{N \cdot l_c}{k_a \cdot \rho} \cdot \frac{c^2}{8} \cdot B_m \cdot \omega \cos(\omega t)$$
$$= I_a\sqrt{1 + \omega^2 k_e^2}\sin(\omega t - \theta_h),\qquad(6)$$

where k_e is a coefficient defined as $\frac{N \cdot l_c}{k_a \cdot \rho} \cdot \frac{c^2}{8} \cdot \frac{B_m}{I_a}$ and $\theta_h = \sin^{-1}\left(\frac{\omega k_e}{1+\omega^2 k_e^2}\right)$ is the phase error caused by the eddy current. Note that the amplitude of the measured current also becomes larger than that of the actual current. The phase error can be rearranged such that

$$\sin\theta_h = \frac{\omega k_e}{\sqrt{1 + \omega^2 k_e^2}}\qquad(7)$$

As k_e has very small value, $\sin\theta_h$ is close to zero. Then, (8) can be approximated such that

$$\theta_h \approx \frac{\omega k_e}{\sqrt{1 + \omega^2 k_e^2}} \approx \frac{\omega k_e}{\sqrt{1}}\qquad(8)$$

The phase shift error increases linearly with ω. The eddy current constant k_e can be calculated once the magnetic core is determined. Equation (5) can be derived when a constant magnetic flux density is distributed throughout the magnetic core of the current transducer. The magnetic core used in this study is constructed by laminating insulated electrical steel sheets. The magnetic field is induced by the primary actual current crossing each sheet of the magnetic core, generating eddy currents. Therefore, the distribution of magnetic flux density within the magnetic core is non-uniform, with the average magnetic flux density slightly decreasing with frequency. The magnetic flux density, accounting for eddy currents, is determined through finite element method (FEM) [6], [15]. In FEM, the shape and the material of a magnetic core are characterized using the properties listed in Table 1, and the core is modeled by laminating sheets. By applying current at various frequencies, the average magnetic flux density of the magnetic core section is calculated when the current reaches its maximum value. Fig. 5 shows the magnetic flux density distribution of the cross section of the magnetic core according to the applied current frequencies.
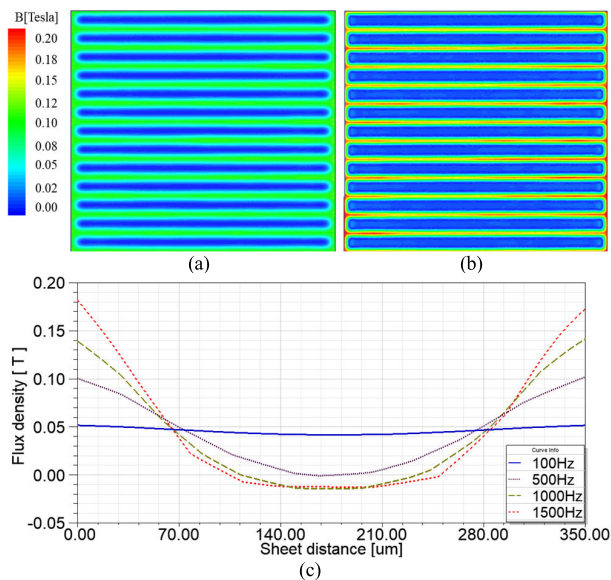
FIGURE 5. Magnetic flux density distribution of the cross section of the magnetic core according to frequency. Depending on frequency (a) 500 Hz, (b) 1.5 kHz, and (c) is flux density distribution in the on sheet.

The eddy current of the magnetic core considering the skin effect depending on the frequency can be expressed as

$$i_e(f) = -\frac{N \cdot l_c \cdot c^2}{8 \cdot \rho \cdot k_a} \cdot \omega \cdot B_{FEM}(f, I_a)\cos(\omega t), \quad (9)$$

where $B_{FEM}(f, I_a)$ is the average magnetic flux density of the magnetic core based on the frequency and the amplitude of the actual current. B_{FEM} can be obtained by using the FEM simulation results as shown in Fig. 5(c). The number

of laminations N of the magnetic core is 38 and the length of magnetic flux path l_c is 82.27 mm used in this paper. Reflecting the skin effect and the stacking factor, k_a is given by 5.28.

The output of the current transducer has an additional component of the eddy current to the primary current. Fig. 6 shows how the eddy current distorts the output of the current transducer as a function of frequency, ranging from 500 Hz to 1.5 kHz, as depicted in (9). The result has the phase error and the amplitude error together. It can be seen that the eddy current increases with frequency and the phase shift error increases accordingly. Table 2 shows $B_{FEM}(f, I_a)$, the phase error, and the amplitude error calculated through FEM when the primary current was injected by a 100 A sinusoidal waveform. I_e is the amplitude of the eddy current.
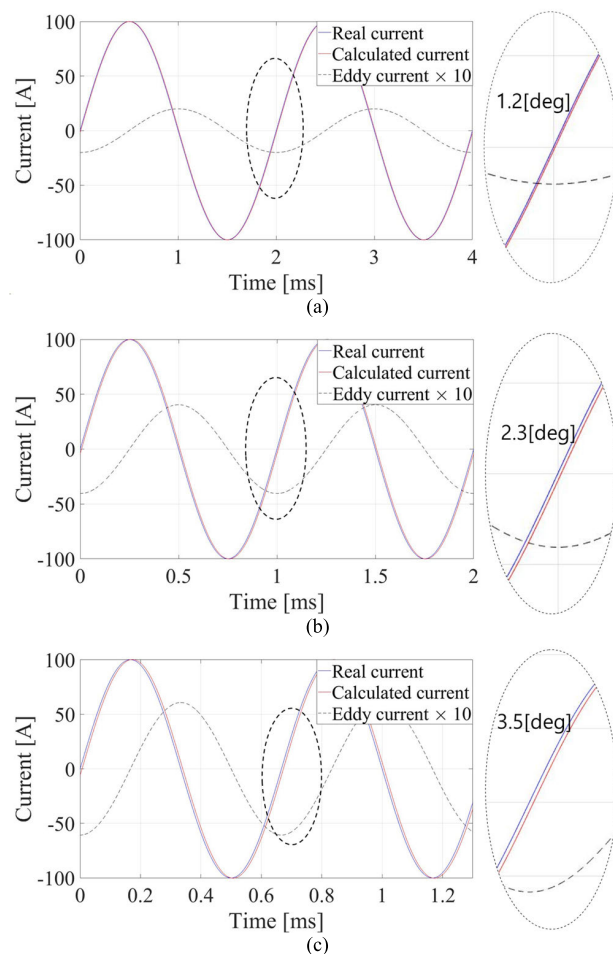
FIGURE 6. The distorted output of the current transducer and calculated depending on frequency (a) 500 Hz, (b) 1 kHz, and (c) 1.5 kHz.

III. COMPENSATION METHOD OF PHASE SHIFT ERROR

A. IMPACT OF CURRENT TRANSDUCER ERROR ON MOTOR CONTROL

To increase the power density of EV powertrain, there are two growing trends: One is to use motors with the higher

TABLE 2. Calculated eddy current and error at 100 A current apply.

Frequency [Hz]	$B_{FEM}(f, I_a)$ [mT]	I_e [A]	Phase error [Degree]	Amplitude error [%]
500	43.0	2.08	1.2	0.02
1000	42.4	4.09	2.3	0.08
1500	41.8	6.14	3.5	0.18

number of poles. The other is to perform field-weakening operations in a speed range more than 3 times higher than the rated speed. Fortunately, the advancement of the wide band-gap (WBG) power semiconductors helps an inverter to increase the fundamental frequency of the motor current. For example, the motor current can be regulated as a sinusoidal waveform above the fundamental frequency of 1 kHz by the use of the pulse width modulation (PWM) frequency at 20 kHz, which is regular value even for high power WBG power semi-conductors [16], [17].

Remind from (6) that the eddy current phenomenon causes the phase shift error and the amplitude error to the measured current. In addition, the phase error should be considered in particular as it is proportional to the frequency of the motor current. On the other hand, the amplitude error is small enough to be ignored. Note that the amplitude error was 0.18% whereas the phase error was 3.5° when the frequency was 1.5 kHz as shown in Table 2. Neglecting the amplitude error of (6), the motor currents can be transformed to the rotating reference frame such that

$$\boldsymbol{i_{dq}} = e^{j\theta_h}\boldsymbol{\hat{i}_{dq}} = \left(\cos\theta_h\hat{i}_d - \sin\theta_h\hat{i}_q\right) + j\left(\sin\theta_h\hat{i}_d + \cos\theta_h\hat{i}_q\right), \quad (10)$$

where $\boldsymbol{i_{dq}}$ is the actual stator currents and $\boldsymbol{\hat{i}_{dq}}$ is the measured currents in the synchronous frame whose d-axis is aligned with the rotor flux. This means that the actual dq-currents leads the measured currents by θ_h. It deteriorates the performance of the vector control and the impact gets more serious during the field-weakening operation.

TABLE 3. Parameter of permanent magnet motor for EV powertrain.

L_d [mH]	L_q [mH]	ψ_m [Wb]	Poles	DC-link Voltage [V]
0.3	0.54	0.1	8	800

Fig. 7 shows how θ_h affects the vector control of an EV traction motor whose parameters are listed in Table 3. The dq-current sets are found analytically to minimize the current amplitudes when producing 100 kW and 200 kW of power over the rated speed. As the actual current set is rotated anti-clockwise by θ_h, the negative i_d should be used excessively. It weakens the rotor field too much thereby reducing the output torque. For example, the current-minimizing solution for 100 kW at 22500 rpm is $i_d = -194.9$ A, $i_q = -48.2$ A. However, even if the inverter precisely regulates the stator currents based on the measured data, $\theta_h = 3.5°$ distorts the

location of actual stator currents as follows: $i_d = -197.5$ A, $i_q = -36.2$ A. It reduces the motor torque by 24.6% from 42.4 Nm to 32.0 Nm.
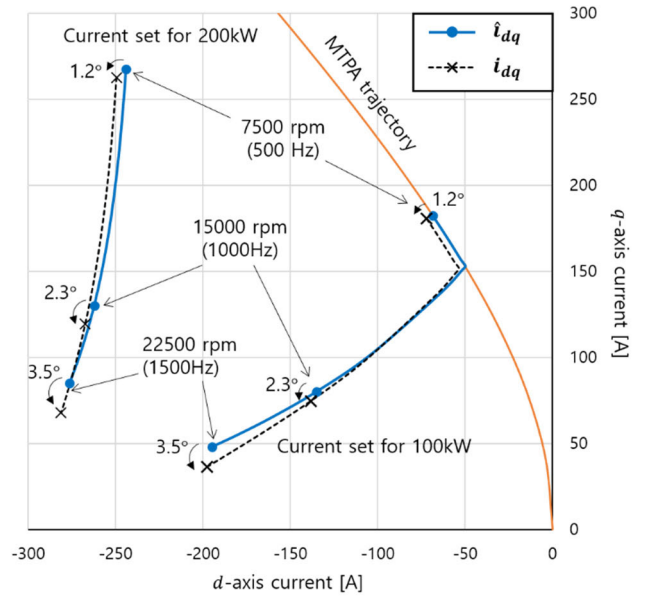
FIGURE 7. Deterioration of dq-current vector control due to θ_h when the motor of EV powertrain is driven from 7500 rpm (500 Hz) to 22500 rpm (1.5 kHz).

As a result, this inherent measurement error of an open-loop current transducer increases the time and the cost to find the entire map of optimal current sets for EV motors. Furthermore, it deteriorates many control algorithms relying on current information like sensorless speed estimator.

Fig. 8 shows the reduction of output torque due to θ_h in the field-weakening operation. When the motor speed was 22500 rpm, torque decreased by 19.5% at 200 kW. The reduction rate increases with the motor speed.
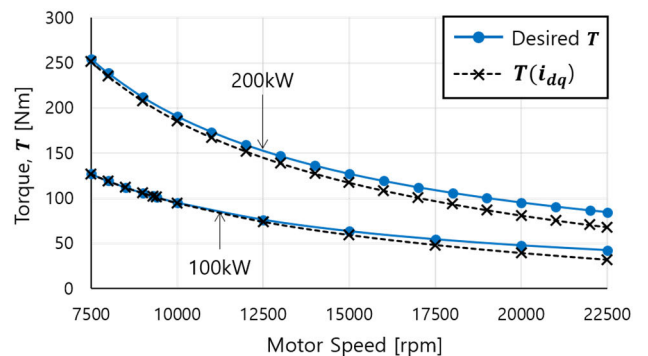
FIGURE 8. Reduction of torque due to θ_h when the motor of EV powertrain is driven from 7500 rpm (500 Hz) to 22500 rpm (1.5 kHz).

B. PROPOSED MOETHOD

As discussed previously, the output error of an open-loop current transducer results in the performance degradation of

the motor control, especially at high speeds. Thus, the phase shift error needs to be corrected. Here, we propose a simple compensation method which utilizes the FEM simulation results.

The phase shift error was approximated as a linear function of the frequency in (8). The coefficient of the linear function, k_e, can be calculated by using the geometric design para-meters of a magnetic core of a current transducer and the flux density as shown in (9). The average flux density is obtained from the FEM simulations. Finally, the electric angle used for the Park transformation from *abc*- to *dq*-currents is corrected as follows

$$\theta_e = \hat{\theta}_e + k_e \cdot 2\pi f, \tag{11}$$

where $\hat{\theta}_e$ is the electric angle measured by a position sensor such as a resolver or an encoder. Fig. 9 shows the block diagram of the current control for the PMSM with the proposed error correction method.
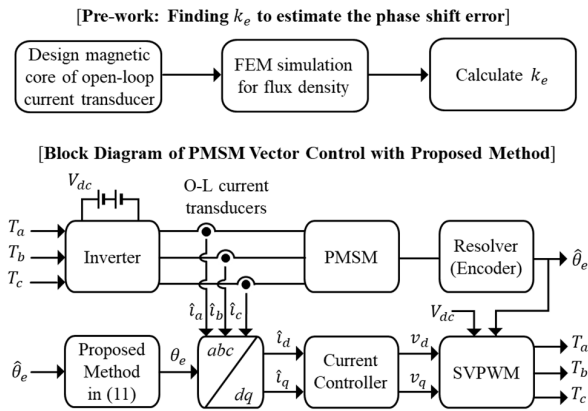

FIGURE 9. Block diagram of phase shift error correction in inverter.

IV. EXPERIMENT RESULTS

The phase shift error of the open-loop current transducer was validated through experiments, with the measurement conducted at the zero crossing point of the actual and measured currents. The actual current is measured by a fluxgate type current transducer. By measuring the output current of the inverter, the proportional relationship between phase shift error and frequency was demonstrated. The power module of the inverter used in the experiment was a silicon carbide FET, CAB530M12BM3 (Wolfspeed). The PWM frequency was set to 20 kHz. A reactor was used for the load. To ensure accurate measurement unaffected by the error, the fluxgate type ITL 900-T (LEM) sensor was utilized, a bandwidth within -1 dB at 100 kHz. The open-loop current transducer employed in this paper has a bandwidth of -3 dB at 40 kHz and is used for motor control. Fig. 10 shows the experimental environment configuration. Open-loop and fluxgate current transducer connected in series to the inverter output [5], [10].

Fig. 11 shows the measured output current of the inverter. The same currents are compared using open-loop and fluxgate current transducers at 500 Hz, 1 kHz, and 1.5 kHz.
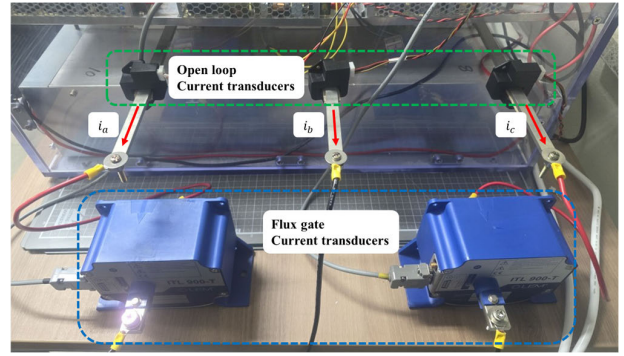

FIGURE 10. Experimental environment (open-loop current transducer and fluxgate current transducer).
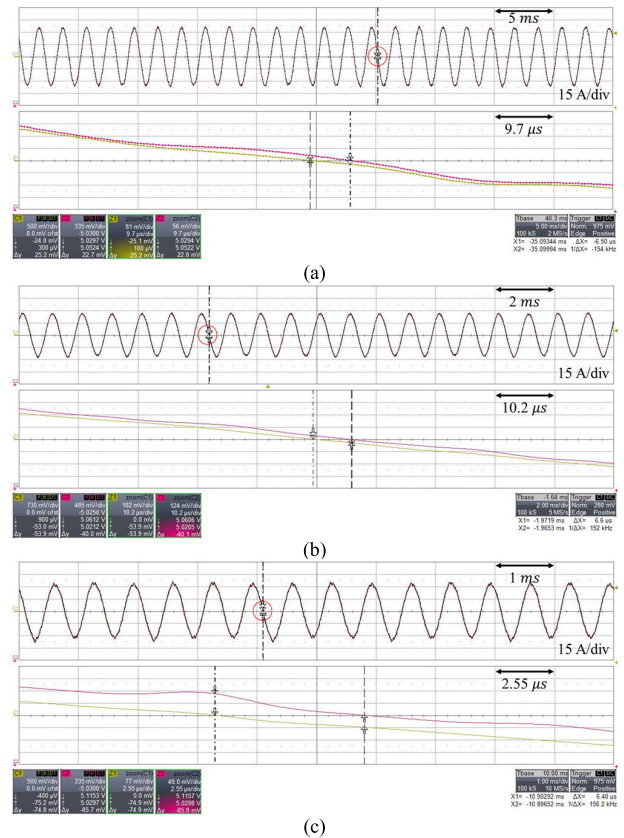

FIGURE 11. Inverter current measurements for open loop current transducer and fluxgate current transducer depending on frequency (a) 500 Hz, (b) 1 kHz, and (c) 1.5 kHz.

The phase shift errors between both current transducers obtained through the experiment are 1.17°, 2.37°, and 3.45°, respectively. Fig. 12 shows the phase shift error for each frequency by calculation result using (11) and experiment result. The compensation coefficient k_e in (11) is obtained as 6.61×10^{-6}. Through the experiment, it was proven that the phase error that occurs is linear and that the eddy current calculation using FEM is valid.

Fig. 13 shows the experimental results of the phase shift error using the analog-to-digital conversion results in the microcontroller, TMS320F28377D (TI). Each waveform is
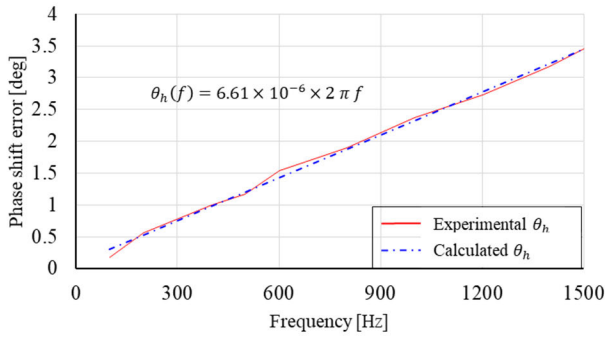
FIGURE 12. Inverter output frequency Vs. phase shift error.

displayed by using the digital to analog conversion (DAC) unit. The green-line denotes data from the fluxgate current transducer, whereas the red-line denotes data from the open-loop current transducer. The results are zoomed at the zero-crossing points as highlighted by red circles. The differences between two waveforms represent the phase shift error of the open-loop current transducers.
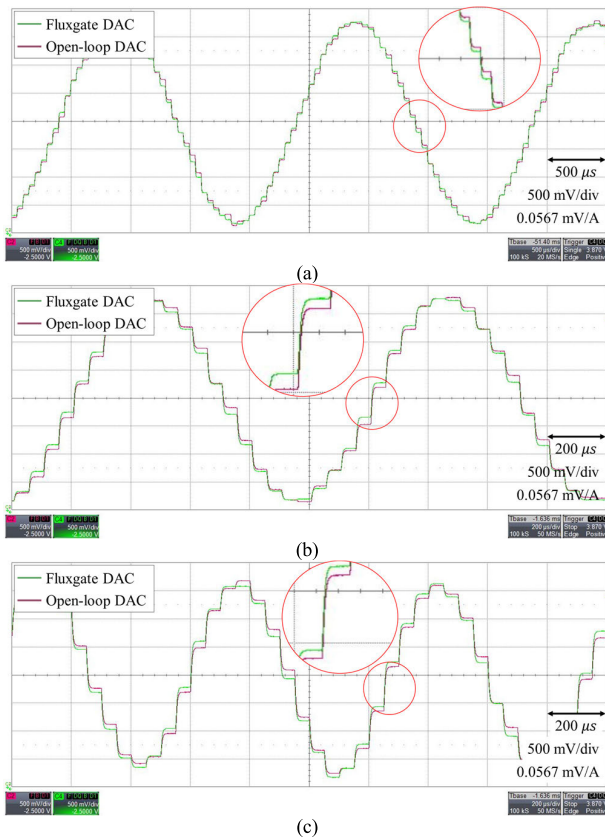

FIGURE 13. DAC current waveform of flux gate and open-loop current transducer measurement current depending on frequency (a) 500 Hz, (b) 1 kHz, and (c) 1.5 kHz.

Fig. 14 shows the experimental results after the phase shift error is corrected by implementing the proposed method to the open-loop current transducer. Note that the differences between the open-loop and the fluxgate current transducer

are reduced significantly so the two waveforms are nearly overlapped. The exact changes of the phase shift error were analyzed using fast Fourier transform (FFT) after restoring the data from the oscilloscope as listed in Table 4. Before implementing the proposed method, the error increases from 0.98° to 3.81° as the frequency of the current increases from 500 Hz to 1500 Hz. After implementing the proposed method, the error was reduced to below 0.2° for all the cases.
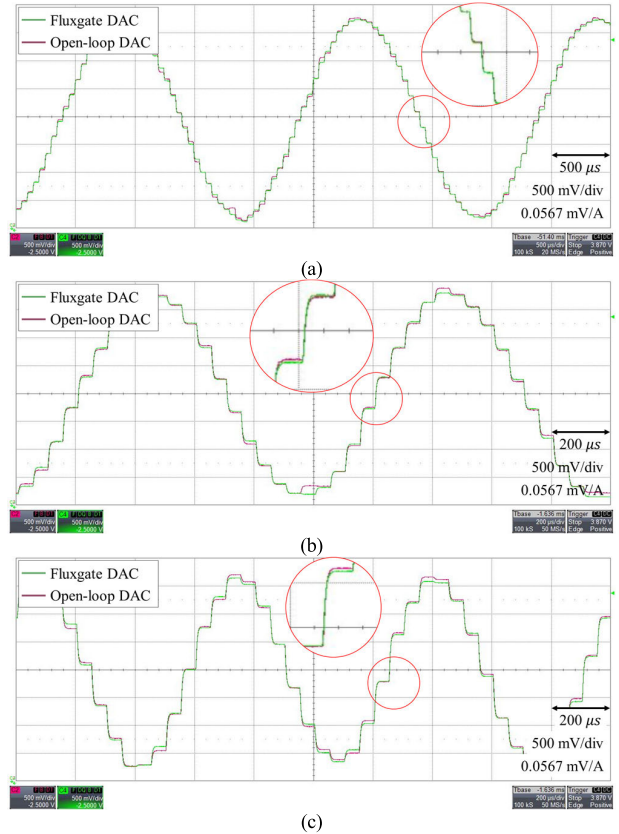

FIGURE 14. Compensated open-loop and flux gate current transducer DAC output waveforms depending on frequency (a) 500 Hz, (b) 1 kHz, and (c) 1.5 kHz.

TABLE 4. Phase shift error correction results obtained by the FFT analysis.

Frequency [Hz]	Before correction Fig. 13 [Degree]	After correction Fig. 14 [Degree]
500	0.98	0.09
1000	2.50	0.15
1500	3.81	0.16

V. CONCLUSION

The open-loop current transducer is widely used in traction inverters. The eddy current induced in the magnetic core of the current transducer generates a measurement error of the phase shift. The relation between the error and the frequency of the current is found by using the mathematical approach and the FEM results together. An approximation method is also applied to simplify the solution. We analyze how this

phenomenon affects the vector control of a motor depending on the frequency of the current. Finally, we propose an online method that corrects the phase shift error using the angular data from a position sensor such as a resolver or an encoder.

The experimental results showed that the phase error is almost linearly proportional to the frequency of the current. A fluxgate current transducer was used for verification. The proposed method well eliminated the phase error for variable frequencies. It will be helpful to improve the performance of the vector control of PMSM, especially for the field-weakening operations.

This work does not fully reflect the effect of the core saturation or the changes in ambient temperature. These nonlinear problems will be studied and verified with the actual motor test setup in the future.

REFERENCES

[1] C. Korasli, "Line-current compensated single toroidal-core current transformer for three-phase current measurement," *IEEE Trans. Power Del.*, vol. 22, no. 1, pp. 500–506, Jan. 2007.

[2] S. Kon and T. Yamada, "Expansion of the impedance and frequency measurement ranges of AC shunt resistors," *IEEE Trans. Instrum. Meas.*, vol. 66, no. 6, pp. 1254–1259, Jun. 2017.

[3] P. Wang, G. Zhang, and Z. Qian, "A planar-coil-based current transducer used in distribution power system," *IEEE Trans. Instrum. Meas.*, vol. 59, no. 11, pp. 3028–3033, Nov. 2010.

[4] K. Kim, H.-P. Sohn, H. Lee, and S.-K. Hong, "A current transducer with digital output for motor drive," *J. Electr. Eng. Technol.*, vol. 17, no. 2, pp. 1371–1378, Mar. 2022.

[5] G. Crotti, D. Gallo, D. Giordano, C. Landi, M. Luiso, C. Cherbaucich, and P. Mazza, "Low cost measurement equipment for the accurate calibration of voltage and current transducers," in *Proc. IEEE Int. Instrum. Meas. Technol. Conf. (I2MTC)*, Montevideo, Uruguay, May 2014, pp. 202–206.

[6] K. Kim, K. Hong, H. Lee, H.-S. Kim, and S.-K. Hong, "Hysteresis compensation method for measurement error of Hall effect current sensor considering eddy current effect for electric vehicle at high speed," in *Proc. IEEE Appl. Power Electron. Conf. Expo. (APEC)*, Anaheim, CA, USA, Mar. 2019, pp. 2653–2658.

[7] M. Roman, G. Velasco, A. Conesa, and F. Jerez, "Low consumption flux-gate transducer for AC and DC high-current measurement," in *Proc. IEEE Power Electron. Specialists Conf.*, Jun. 2008, pp. 535–540.

[8] D. Jobling, "New open-loop current transducers with near closed-loop performance," in *Proc. Int. Exhib. Conf. Power Electron., Intell. Motion, Renew. Energy Energy Manage.*, Nuremberg, Germany, May 2014, pp. 1–5.

[9] H. Hwang, D. Park, W. Lee, K. Hong, and K. Kim, "Mathematical models with temperature compensation for InSb and GaAs Hall sensors using linear regression method," in *Proc. Int. Conf. Electron., Inf., Commun. (ICEIC)*, Honolulu, HI, USA, Jan. 2018, pp. 1–4.

[10] K. Kim, H.-S. Seo, H. Lee, and S.-K. Hong, "Comparison of current transducer characteristics according to electrical steel magnetic core materials," in *Proc. 24th Int. Conf. Electr. Mach. Syst. (ICEMS)*, Oct. 2021, pp. 2415–2418.

[11] X. Cheng, Z. Zhang, F. Li, and S. Liu, "Study of magnetic properties for iron core in a closed loop Hall current sensor," in *Proc. 13th Int. Conf. Electron. Packag. Technol. High Density Packag.*, Guilin, China, Aug. 2012, pp. 575–578.

[12] M. Taghizadeh Kakhki, J. Cros, and P. Viarouge, "New approach for accurate prediction of eddy current losses in laminated material in the presence of skin effect with 2-D FEA," *IEEE Trans. Magn.*, vol. 52, no. 3, pp. 1–4, Mar. 2016.

[13] L. Cristaldi, A. Ferrero, M. Lazzaroni, and R. T. Ottoboni, "A linearization method for commercial Hall-effect current transducers," *IEEE Trans. Instrum. Meas.*, vol. 50, no. 5, pp. 1149–1153, Oct. 2001.

[14] D. Ribbenfjard and G. Engdahl, "Novel method for modelling of dynamic hysteresis," *IEEE Trans. Magn.*, vol. 44, no. 6, pp. 854–857, Jun. 2008.

[15] M. S. S. Nia, S. Saadatmand, M. Altimania, P. Shamsi, and M. Ferdowsi, "Analysis of skin effect in high frequency isolation transformers," in *Proc. North Amer. Power Symp. (NAPS)*, Wichita, KS, USA, Oct. 2019, pp. 1–6.

[16] M. Nitzsche, C. Cheshire, M. Fischer, J. Ruthardt, and J. Roth-Stielow, "Comprehensive comparison of a SiC MOSFET and Si IGBT based inverter," in *Proc. Int. Exhib. Conf. Power Electron., Intell. Motion, Renew. Energy Energy Manage.*, Nuremberg, Germany, May 2019, pp. 1–7.

[17] A. Albanna, A. Malburg, M. Anwar, A. Guta, and N. Tiwari, "Performance comparison and device analysis between Si IGBT and SiC MOSFET," in *Proc. IEEE Transp. Electrific. Conf. Expo (ITEC)*, Dearborn, MI, USA, Jun. 2016, pp. 1–6.

KISEOK KIM (Graduate Student Member, IEEE) received the B.S. and M.S. degrees in system control engineering and information control engineering from Hoseo University, South Korea, in 2015 and 2017, respectively, where he is currently pursuing the Ph.D. degree in information control engineering.

From 2017 to 2022, he was an Associate Research Engineer with the ITX-AI Company Ltd. Since 2023, he has been the Research and Development Manager with ELEXSEN Corporation. He holds a patent related to current measurement. His research interests include electromagnetic analysis, current measurement, current control of power electronics systems, traction motor drives, and high-power inverters.

YOONJAE KIM (Member, IEEE) received the B.S. degree in electrical engineering from Sungkyunkwan University, Suwon, South Korea, in 2012, and the Ph.D. degree in electrical engineering from Pohang University of Science and Technology, Pohang, South Korea, in 2018. From 2018 to 2021, he was a Staff Engineer with Samsung Electronics, Suwon. Since 2021, he has been an Assistant Professor with the Department of Electrical Engineering, Hoseo University, Asan, South Korea. His research interests include design and control of ac motors, and various power electronics in industrial fields.

JI-HOON HAN (Graduate Student Member, IEEE) received the B.S. and M.S. degrees in digital control engineering and information control engineering from Hoseo University, South Korea, in 2019 and 2021, respectively, where he is currently pursuing the Ph.D. degree in information control engineering.

He is currently an Instructor with Hoseo University. His research interests include deep learning, motor design, and electromagnetic field analysis.

SUN-KI HONG (Member, IEEE) received the B.S., M.S., and Ph.D. degrees in electrical engineering from Seoul University, South Korea, in 1987, 1989, and 1993, respectively. In 1995, he joined Hoseo University, where he is currently a Full Professor with the Department of System and Control Engineering. His research interests include hysteresis motor analysis, electric motor analysis and design, motor fault diagnosis, servo motor control, converter and inverter design, deep learning, and the IoT.

• • •